Plastic design of stainless steel continuous beams

Michaela Gkantou, Georgios Kokosis, Marios Theofanous and Samir Dirar

University of Birmingham, School of Engineering, Department of Civil Engineering, UK

Abstract

In this paper an experimental study on eight simply-supported and four two-span continuous beams employing austenitic and duplex stainless steel rectangular hollow sections (RHS) is reported. In parallel with the tests, finite element models were developed. Upon validation against the experimental results, parametric studies were conducted to expand the available structural performance data over a range of cross-section slendernesses, structural systems and load configurations likely to occur in practice. The obtained experimental and numerical results along with collated test data were used to assess the accuracy of EN 1993-1-4 design provisions and to explore the possibility of plastic design for stainless steel indeterminate structures, simultaneously accounting for the effect of strain-hardening at cross-sectional level and moment redistribution exhibited by structures employing stocky cross-sections.

Keywords

Stainless steel structures; Continuous beams; Plastic design; Eurocode 3; Continuous Strength Method (CSM)

1   Introduction

The excellent atmospheric corrosion resistance and favourable mechanical properties of stainless steel make it well suited for a range of structural applications, particularly in aggressive environments or where durability and low maintenance costs are crucial design criteria [1, 2]. The main disadvantage hindering the more widespread usage of stainless steel in construction is its high material cost and price volatility. However, life-cycle costing [3] and sustainability considerations [4] make stainless steels more attractive when cost is considered over the full life of the project, due to the high potential to recycle or reuse the material at the end of life of the project.

The design of stainless steel structures is covered by a number of international design codes [5-8], which have either recently been introduced [8] or were recently amended [5-7] in light of recent experimental tests, thus indicating the worldwide interest stainless steel has received in recent years. Despite the absence of a well-defined yield stress, all current design standards for stainless steel adopt an equivalent yield stress and assume bilinear (elastic, perfectly-plastic) behaviour for stainless steel as for carbon steel in an attempt to maintain consistency with traditional carbon steel design guidance. Neglecting the significant strain-hardening inherent in stainless steel has been shown to lead to overly conservative design, particularly for stocky stainless steel components [9-13]. Given the high material cost of stainless steel, improving existing design guidance is warranted. Improvements can be made either by calibrating the existing design procedures, some of which are based on engineering judgment and limited test data, against additional experimental results, or by devising more accurate design approaches in line with the actual material response. In any case more efficient yet safe design rules are desirable. To this end, the classification limits for stainless steel elements have been revised on the basis of a collection of all available test results [14] and were included in the recently amended version of EN 1993-1-4 [5]. Moreover the development of the Continuous Strength Method [15] as a rational means to account for the significant strain-hardening exhibited by stocky sections in design led to its incorporation as an alternative design approach in [8]. Similarly, research

on the structural response of slender stainless steel sections has led to the extension of the Direct Strength Method to stainless steel compression members [16].

The majority of published research articles on stainless steel structures focus on the response of individual members. All published literature on the behaviour of stainless steel indeterminate structures is limited to five publications [17-21], which investigate the structural response of two-span continuous beams subjected to point loads. It was established that for austenitic and duplex stainless steels both strain-hardening at cross-sectional level and moment redistribution for indeterminate structures employing stocky sections have to be allowed for in design and that the current design guidance severely underestimates the load carrying capacity of stainless steel indeterminate structures employing Class 1 sections by 40% on average [19]. However, due to insufficient relevant experimental data, no rules are given for plastic global analysis of indeterminate stainless steel structures in any current structural design code, even though the ductility of stainless steel is superior to that of ordinary structural steel. Large inelastic rotations and large strains can clearly be accommodated by sufficiently stocky stainless steel sections [9, 11, 13].

The controversy of not allowing plastic design for an indeterminate structure made of a ductile material is obvious in [5] where it is explicitly stated that "No rules are given for plastic global analysis" even though a slenderness limit for Class 1 elements is specified in the same code. Deficiencies in current design guidance put stainless steel at a disadvantage compared to other materials. Due to a gap in current knowledge, the design standards for stainless steel impose strict restrictions to its design, thereby hindering its use in applications where it appears as the preferred solution. To address the lack of design guidance on global plastic design of stainless steel structures, a research project investigating the response of stainless steel continuous beams and frames is currently underway at the University of Birmingham. This paper reports a series of tests on simply-supported beams, which are utilized to establish the cross-sectional response under bending both in absence and in the presence of moment gradient and a series of tests on continuous stainless steel beams. In parallel, finite element (FE) models were developed and validated against the experimental results and parametric studies were conducted to expand the available structural performance data over a range of cross-section slendernesses, structural systems and load configurations likely to occur in practice. The obtained experimental and numerical results were used to assess the accuracy of EN 1993-1-4 [5] and to explore the possibility of plastic design for stainless steel continuous beams.

2   Experimental studies

Physical tests were carried out on simply-supported beams loaded in the 3-point bending and in the 4-point bending configuration and on two-span continuous beams loaded with point loads at their mid-span in the Structures Lab at the University of Birmingham. In addition, tensile tests on flat and corner coupons extracted from the finished cross-sections were carried out in the lab of the department of Metallurgy and Materials at the University of Birmingham.

2.1   Chosen cross-sections

Four rectangular hollow sections (RHS) with a nominal outer web depth H and a nominal outer flange width B equal to 100 mm and 50 mm respectively were employed in the experimental study reported herein. The employed sections cover not only a wide range of local slendernesses, but also different material grades and production techniques. Three of the sections were cold-formed from Grade EN 1.4301/1.4307 austenitic stainless steel and had a nominal thickness t of 2 mm, 3 mm and 5 mm. The fourth section was fabricated by welding two parallel flange channel sections cold-formed from Grade 1.4462 duplex stainless steel along the flange tips and had a nominal thickness of 3 mm. Hence the austenitic cold-formed RHS had a seam weld along the centreline of one of the webs (i.e. longer faces), whilst the fabricated duplex RHS had a longitudinal weld along the centreline of each flange. It is noteworthy that the welded duplex section was fabricated due to difficulties associated with sourcing cold-formed duplex stainless steel RHS in small quantities (as required for a research project), whilst austenitic stainless steel RHS were readily available. Moreover, despite the lower nickel content which is expected to lead to a lower price [22], lean duplex stainless steels were even more expensive than their ordinary

duplex counterparts, unless a large quantity was requested. Clearly several issues with the supply chain need to be addressed to take advantage of the benefits of such novel structural materials. Prior to testing, careful measurements were taken for each beam specimen. Since all beam specimens for each section were cut from the same length of tubes, the measurements were averaged for each nominal cross-section and are reported in Table 1, where r_i refers to the internal corner radius and the remaining symbols have been previously defined. The subscript D following the section designation denotes the specimen in duplex stainless steel.

Table 1. Mean measured dimensions of tested cross-sections

Cross-section	Material Grade	B (mm)	H (mm)	t (mm)	r_i (mm)
RHS $100 \times 50 \times 2$	EN 1.4301/1.4307	50.04	100.13	1.90	1.70
RHS $100 \times 50 \times 3$	EN 1.4301/1.4307	49.97	100.17	2.90	2.25
RHS $100 \times 50 \times 5$	EN 1.4301/1.4307	50.19	100.42	4.93	2.56
RHS $100 \times 50 \times 3$-D	EN 1.4462	50.19	100.44	2.87	2.56

2.2   Material coupon tests

Two flat material coupons (i.e. one from the mid-width of the web and one from the mid-width of the flange) and one corner coupon were extracted from each of the four cross-sections considered herein and were tested according to EN ISO 6892-1 [23]. A pronounced curving of the coupons was observed upon their extraction due to the release of bending residual stresses. The residual stresses were reintroduced upon gripping the coupons between the jaws of the testing machine upon application of small gripping loads. Hence it is assumed that the obtained stress-strain response inherently includes the effect of bending residual stresses. The obtained results are summarized in Table 2, where E is the Young's modulus, $\sigma_{0.2}$ is the 0.2 % proof stress, $\sigma_{1.0}$ is the 1.0 % proof stress, σ_u is the ultimate tensile stress, ε_f is the plastic strain at fracture and n and $n_{0.2,1.0}$ are material parameters used in the two-stage Ramberg-Osgood [17, 24, 25] material model, which is adopted in the numerical modelling as discussed in the next section. Typical stress-strain curves are depicted in Fig.1(a) for the RHS $100 \times 50 \times 2$ and the duplex RHS $100 \times 50 \times 3$ material coupons, where the corner coupons are seen to possess enhanced material strength. Typical coupons before, during and after testing are shown in Fig.1(b).

Table 2. Tensile coupon test results

Specimen	E (N/mm^2)	$\sigma_{0.2}$ (N/mm^2)	$\sigma_{1.0}$ (N/mm^2)	σ_u (N/mm^2)	ε_f	Compound R-O coefficients	
						n	$n_{0.2,1.0}$
RHS $100 \times 50 \times 5$ Flange	190000	481	533	746	0.55	8.5	3.25
RHS $100 \times 50 \times 5$ Web	201700	490	535	758	0.54	8.0	3.25
RHS $100 \times 50 \times 5$ Corner	198000	697	800	839	0.48	10.0	3.80
RHS $100 \times 50 \times 3$ Flange	200600	458	507	699	0.57	8.0	2.90
RHS $100 \times 50 \times 3$ Web	193800	473	506	698	0.58	10.0	2.30
RHS $100 \times 50 \times 3$ Corner	201000	510	626	698	0.46	6.0	3.90
RHS $100 \times 50 \times 2$ Flange	193800	450	482	774	0.55	9.0	2.25
RHS $100 \times 50 \times 2$ Web	200600	434	473	769	0.56	8.0	2.20
RHS $100 \times 50 \times 2$ Corner	203000	545	650	809	0.34	6.0	4.50
RHS $100 \times 50 \times 3$ Flange-D	203600	576	643	822	0.34	12.0	2.50
RHS $100 \times 50 \times 3$ Web-D	198300	582	637	808	0.29	12.0	2.50
RHS $100 \times 50 \times 3$ Corner-D	190000	718	840	893	0.24	6.0	4.75
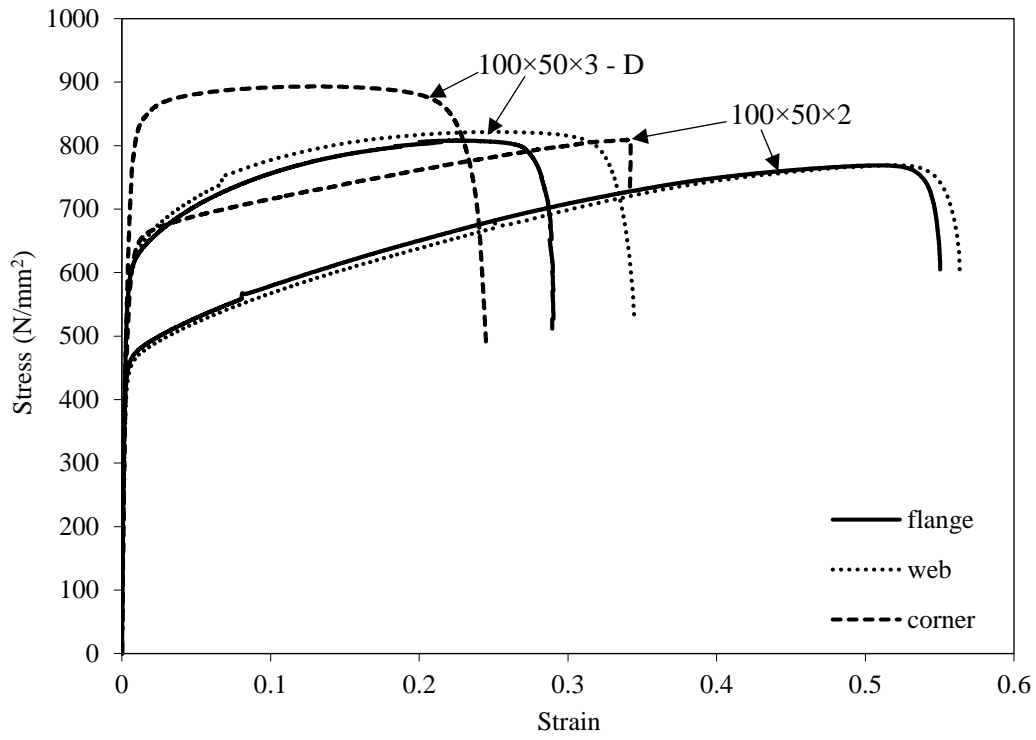
a) Stress-strain curves

Flat coupon 100×50×2

Corner coupon 100×50×5

100×50×3 web   100×50×5 flange   100×50×5 corner

b) Tested coupons

Fig.1. Flat and corner tensile coupons

The key material properties stated in the mill certificates for the sheet material used for the fabrication of the cross-sections are summarized in Table 3. As expected the proof stress and ultimate stress values corresponding to coupons extracted from the finished sections are significantly higher compared to the mill certificate values for the austenitic cross-sections, since during the cold-forming production process the coil material properties are significantly enhanced [26]. A far inferior level of enhancement can be observed for the duplex cross-sections, arguably due to the different fabrication process.

Table 3. Material properties according to mill certificates

| Cross-section	Material Grade	$\sigma_{0.2}$ (N/mm^2)	$\sigma_{1.0}$ (N/mm^2)	σ_u (N/mm^2)	ε_f %
RHS $100 \times 50 \times 2$	EN 1.4307/1.4301	324	356	634	54
RHS $100 \times 50 \times 3$	EN 1.4307/1.4301	312	348	625	55
RHS $100 \times 50 \times 5$	EN 1.4307/1.4301	310	351	639	54
RHS $100 \times 50 \times 3$	EN 1.4462	555	-	765	32

2.3 Tests on simply-supported beams

For each of the four cross-sections, one beam was tested in the 3-point bending configuration and one in the 4-point bending configuration to study the response in major axis bending. The test arrangement and employed instrumentation for the 3-point bending tests is schematically shown in Fig.2, whilst the overall setup is depicted in Fig.3. All specimens had a total length of 1500 mm and the simply-supported conditions were achieved with the use of steel rollers, which allowed both the rotation about the axis of bending and the axial displacement at the ends of the beams. The rollers were placed 75 mm inwards from each beam end, as a result the span of the beams was 1350 mm as shown in Fig.2. In order to prevent web crippling [27], wooden blocks which were closely matching the dimensions of the tested beams, were inserted into the tubular specimens at the loading point and the supports.
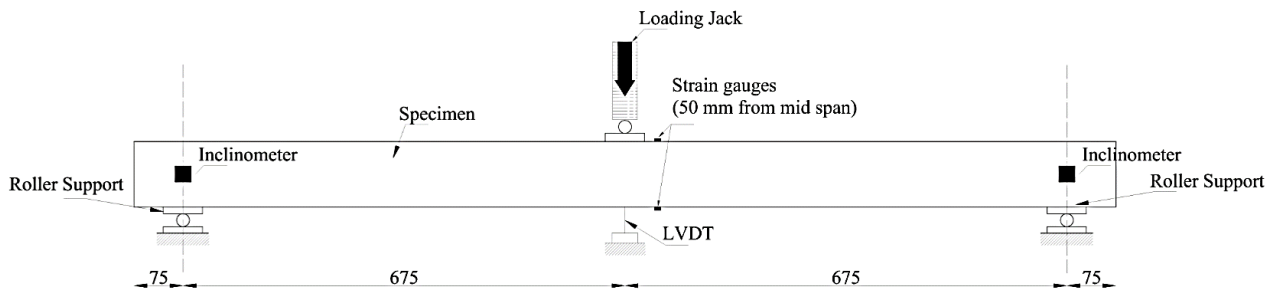
Fig.2. Schematic 3-point bending test arrangement and instrumentation (dimensions in mm)

Fig.3. Overall setup for 3-point bending tests

All beams tested in the 3-point bending configuration were loaded at mid-span by a hydraulic actuator at a rate of 1.5 mm/min. Two inclinometers were placed at the supports, as shown in Fig.2, in order to measure the end-rotations of the 3-

point bending tests. For each specimen, two strain gauges were attached, one at the top and one at the bottom flange, at a distance of 50 mm from the loading point, in order to measure the extreme tensile and compressive strains that occur during the bending tests. Moreover, one linear variable displacement transducer (LVDT) was located at the loading point of the 3-point bending tests, in order to measure the vertical deflection of the mid-span. The Squirrel data logger was used for recording the load, strains, end-rotations and mid-span displacements at 2 sec intervals.

The 4-point bending test arrangement was similar to the 3-point bending one, as shown schematically in Fig.4. Two equal point loads were applied at a distance equal to one-third of the clear span length from each end support via a spreader beam, which was positioned between the loading jack and two steel rollers, resting on the top flange of the specimens at the loading points and loaded at mid-span via a hydraulic actuator. As with the 3-point bending tests, wooden blocks were inserted within the tubes at the two loading points and supports to prevent web crippling.
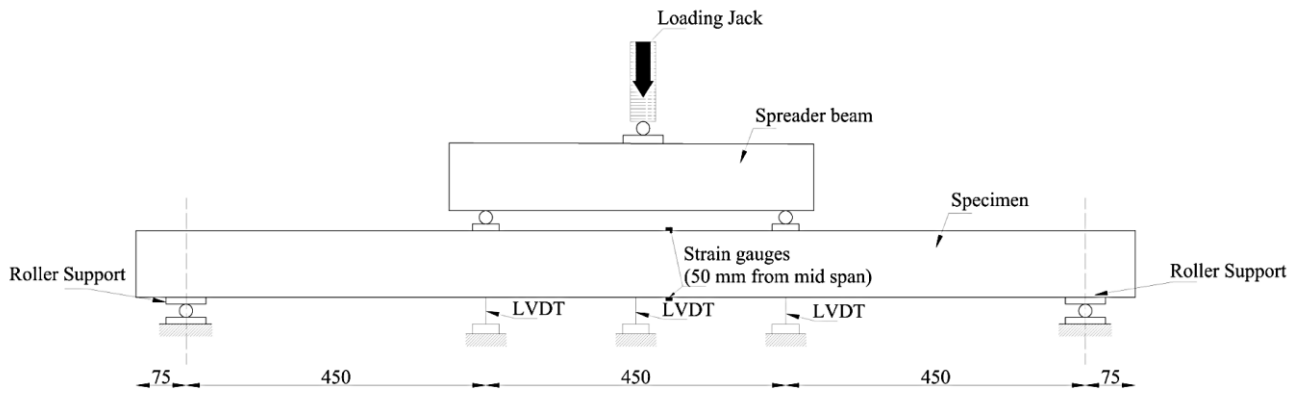
Fig.4. Schematic 4-point bending test arrangement and instrumentation (dimensions in mm)

In Fig.5 the moment-rotation and moment-curvature response of all specimens are depicted for the 3-point bending and 4-point bending tests respectively. To facilitate the comparison between the responses exhibited by the tested sections, the curves are displayed in a non-dimensional format, where the moments are normalized by the plastic moment resistance M_{pl} and the rotations θ or curvatures k are normalized by the elastic part of the rotation θ_{pl} or the elastic part of the curvature k_{pl} corresponding to M_{pl} on the ascending branch, as shown in Fig.5. The definitions of the elastic part of the rotation and the curvature are given in Equations (1) and (2) respectively. In these formuli, I is the second moment of area of the section, L the span's length and M_{pl} the plastic moment resistance evaluated using the average $\sigma_{0.2}$ values, as obtained for the material coupon tests (see Table 2).
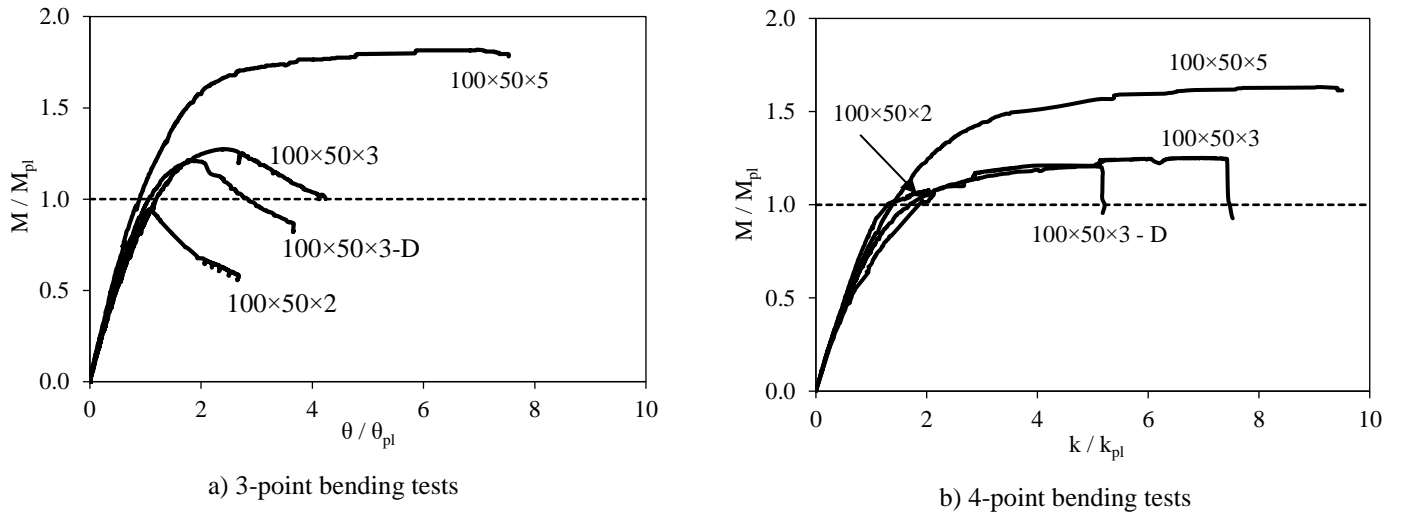
$$\theta_{pl} = \frac{M_{pl}L}{2EI} \tag{1}$$
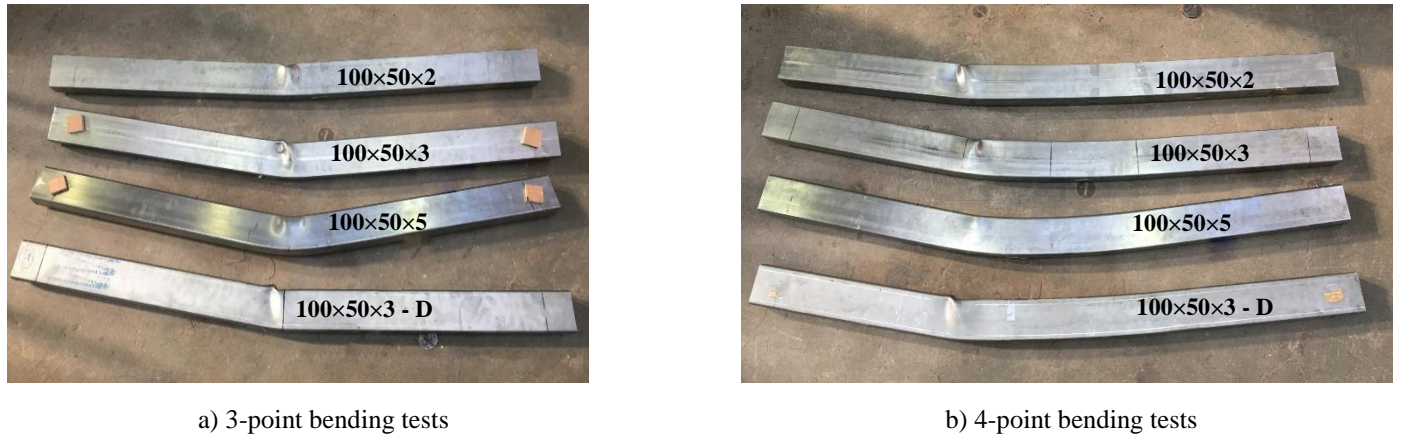
$$k_{pl} = \frac{M_{pl}}{EI} \tag{2}$$

Key experimental results, including the moment resistance M_u, the ratios of the ultimate moment to the elastic and plastic moment resistance (M_u/M_{el} and M_u/M_{pl} respectively) and the rotation capacity R are reported in Table 4. The rotation capacity is defined by Equation (3), where θ_u (k_u) refers to the total rotation (total curvature) at mid-span when the moment-rotation (moment-curvature) curve falls back below M_{pl}, as obtained from the tests. No rotation capacity is defined for specimens failing prior to reaching M_{pl}. All failed specimens are depicted in Fig.6. All failure modes relate to local buckling of the compression flange and the upper part of the web.

$$R = \frac{\theta_u}{\theta_{pl}} - 1 \; ; \qquad\qquad R = \frac{k_u}{k_{pl}} - 1 \qquad\qquad\qquad (3)$$

a) 3-point bending tests

b) 4-point bending tests

Fig.5. Normalized moment-rotation and moment-curvature response

a) 3-point bending tests

b) 4-point bending tests

Fig.6. Failure modes for 3-point bending and 4-point bending tests

Table 4. Key experimental results from 3-point and 4-point bending tests

Cross-section	Test configuration	M_u (kNm)	M_u/M_{el}	M_u/M_{pl}	R
RHS $100 \times 50 \times 2$		7.41	1.18	0.96	N/A
RHS $100 \times 50 \times 3$	3-point bending	15.51	1.59	1.28	3.23
RHS $100 \times 50 \times 5$		36.86	2.33	1.82	6.53
RHS $100 \times 50 \times 3$-D		18.08	1.50	1.20	1.76
RHS $100 \times 50 \times 2$		8.46	1.35	1.10	0.48
RHS $100 \times 50 \times 3$	4-point bending	15.21	1.56	1.25	6.46
RHS $100 \times 50 \times 5$		33.08	2.09	1.63	8.51
RHS $100 \times 50 \times 3$-D		18.13	1.51	1.21	4.21

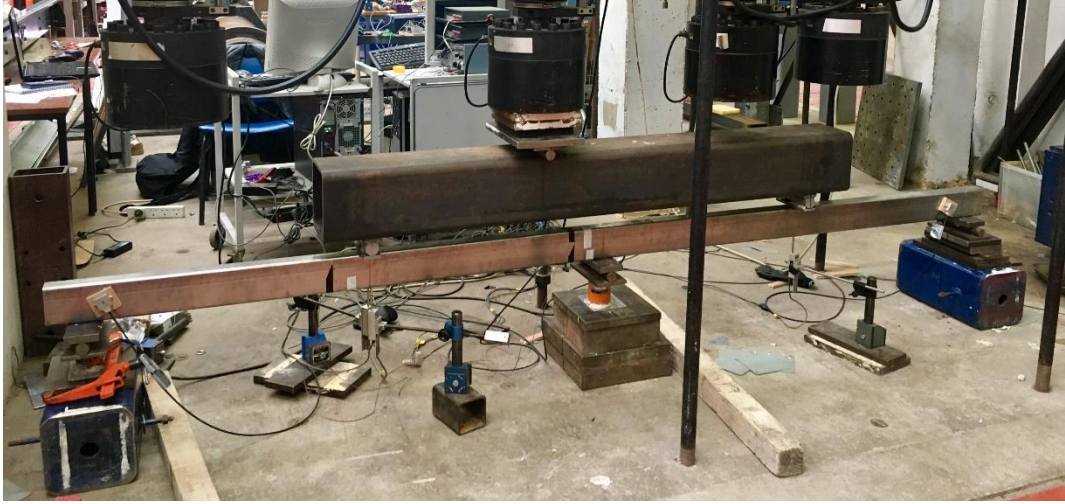## 2.4   Tests on continuous beams

In order to determine the redistribution capacity of austenitic and duplex stainless steel continuous beams, four two-span structural configurations were subsequently conducted on the same cross-section sizes and material employed for the simply-supported beams, considering the case of major axis bending only. All specimens had a total length of 3000 mm. Preliminary investigations were conducted in order to find a loading configuration that would allow significant moment redistribution. An insight in the structural response of stainless steel beams was offered by testing continuous beams with one of the two equal spans having twice the load of the other (i.e. one span loaded with a concentric load "P/3" and the other one with "2P/3", where P the reference total load). In this way, the first plastic hinge would develop at the loading point "2P/3" followed by a second one at the central support. The sequence of the plastic hinge formation is hence reverse from that studied previously in [17-21].

The continuous beam test arrangement is shown schematically in Fig.7. The simply-supported conditions were achieved with the use of steel rollers at the three supports. The clear span between the supports was 1425 mm. The instrumentation included two load cells, four inclinometers, four strain gauges and two LVDTs. The load cells were used to measure the reaction forces. The inclinometers were used to measure the rotations in the two end supports and in the two sides of the central support. The strain gauges were affixed at a distance 50 mm from the central support and from the "2P/3" loading point and their readings were used to ensure that no axial restraint was provided by the end rollers. The LVDTs were used to record the two vertical mid-span displacements. Similarly to the simply-supported beams, in order to prevent web crippling failure, wooden blocks were inserted in the tubular specimens at the loading points and the supports. In order to prevent local bearing failure, steel blocks of 15 mm thickness were used for the application of the load and at the end rollers. A spreader beam eccentrically loaded, as shown in Fig.7, was used to ensure the required loading configuration. The load was assigned vertically with a loading rate of 1.5 mm/min. The Squirrel data logger was used for recording the load, strains, end-rotations, reaction forces and mid-span displacements at 2 sec intervals. A photograph from the overall set up is given in Fig.8.
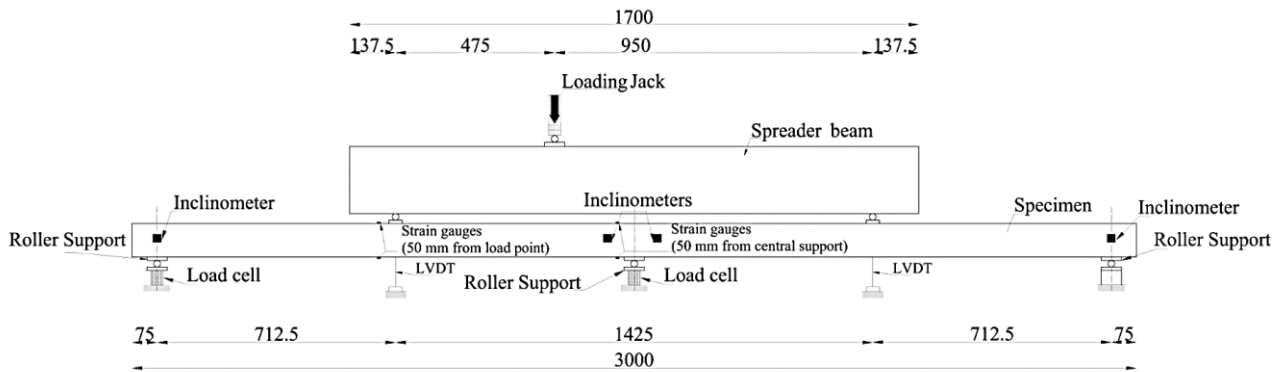
Fig.7. Schematic continuous beam test arrangement and instrumentation (dimensions in mm)
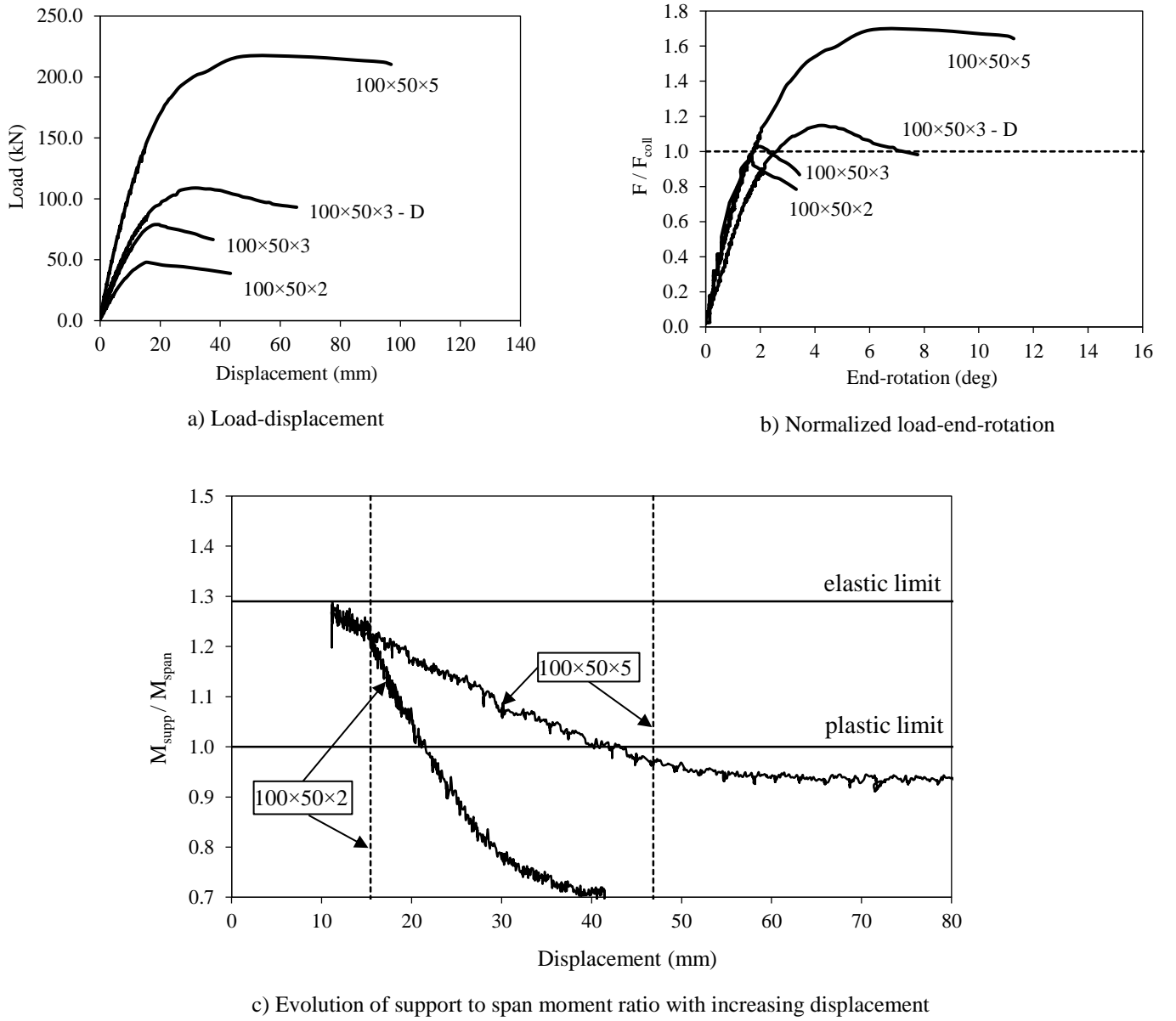
Fig.8. Overall setup for continuous beam tests

The key results are summarized in Table 5, where F_u is the experimental load at collapse, δ_u is the vertical displacement at "2P/3" loading point at collapse, θ_u is the end-rotation of the most heavily loaded span at collapse and F_{coll} is the theoretical plastic collapse load evaluated in line with classical plastic analysis procedures, considering rigid-plastic material response. As anticipated, all specimens failed by developing a distinct plastic hinge at "2P/3" loading point, followed by a second plastic hinge at the central support. The experimental response is shown in Fig.9(a), where the load is plotted against the vertical displacement at "2P/3" loading point for all four specimens. The load normalized by the F_{coll} is plotted against the end-rotation in Fig.9(b). The evolution of the support to span moment ratio (M_{supp}/M_{span}) against the increasing vertical displacement at "2P/3" loading point is shown in Fig.9(c) for the most slender and the stockiest specimen. The horizontal lines of 1.29 and 1.0 correspond to the theoretical moment ratios of the elastic and rigid plastic analysis respectively and the vertical lines pass through the displacement at which the ultimate load occurred. As can be seen for the stockiest 100×50×5 specimen, the moment ratio is equal to the elastic ratio at the initial stages of loading and falls to unity (i.e. the plastic ratio) at the ultimate load, after yielding, plastic spreading and moment redistribution has taken place. The specimen 100×50×2 failed in smaller strains, before significant moment redistribution had occurred. Given that the aforementioned specimen achieved very small deformation capacity in the respective 4-point test, this response was anticipated. Note that as will be discussed in Section 4, this is a Class 2 section according to Eurocode [5] (i.e. not aimed for plastic design).

Table 5.   Key results from continuous beam tests

Cross-section	Class [5]	F_u (kN)	F_{coll} (kN)	δ_u (mm)	θ_u (deg)
RHS $100 \times 50 \times 2$	2	47.94	48.66	15.44	1.59
RHS $100 \times 50 \times 3$	1	78.85	76.73	19.55	2.01
RHS $100 \times 50 \times 5$	1	216.60	128.04	46.86	6.02
RHS $100 \times 50 \times 3$-D	1	108.86	94.88	30.95	4.16

a) Load-displacement

b) Normalized load-end-rotation

c) Evolution of support to span moment ratio with increasing displacement

Fig.9. Continuous beam tests results

3   Numerical modelling

3.1   Development of FE models

Finite element models were developed using the general purpose FE software ABAQUS [28]. The reduced integration 4-noded shell element S4R suitable for thin or thick shell applications with finite membrane strains was used throughout this study. Mesh convergence studies revealed that a uniform mesh with a size equal to the element thickness for the flat parts of the sections and 3 elements per curved corner region provided a good balance between accuracy and computational cost and were adopted for all simulated sections. To increase computational efficiency, the symmetry with respect to boundary conditions, loading and failure mode was exploited and only half the cross-section was modelled with suitable symmetry boundary conditions applied along the plane of symmetry. The remaining boundary conditions applied were in agreement with the support conditions employed in the tests, whilst the effect of the wooden blocks introduced in the locations of point loads application and support reactions to prevent local bearing failure was simulated by applying the distributing coupling constrain.

Material nonlinearities were accounted for using the von Mises yield criterion and isotropic hardening plasticity. The experimentally derived stress-strain curves (see Section 2.2) were converted into the true stress-logarithmic plastic strain format and input into the FE models. Corner strength enhancements brought about by the cold-forming process, by which

10

the sections were produced, were explicitly simulated by assigning the experimentally derived corner properties to the corner regions. In agreement with similar studies [22], the corner properties were assumed to extend into the adjacent flat parts by a width equal to two times the section thickness.

Initial geometric imperfections in the form of the lowest elastic buckling mode shape were assumed to be a suitable representation of the geometric imperfections inherently present in structural members. To this end, an eigenvalue buckling analysis was initially conducted and the obtained lowest buckling mode shapes consistent with local buckling over the points of load application and support reactions were introduced in the subsequent geometrically and materially nonlinear analysis. Three imperfection amplitudes, equal to t/10, t/50 and t/100, where t is the thickness of the simulated section, were considered. Residual stresses were not explicitly modelled; the effect of bending residual stresses is assumed to be reflected in the adopted material properties, as previously discussed, whilst membrane residual stresses of cold-formed sections have been found small compared to the bending ones [22] and their effect was not accounted for in the numerical investigation. The same assumptions have been successfully applied in past research [22].

3.2 Validation of FE models

Following the aforementioned modelling assumptions, the numerical results are compared with the experimental ones for the purposes of validation. Table 6 shows the numerical over experimental ultimate load ratios for the geometric imperfection amplitudes considered. Typical load-deformation curves are shown in Fig.10, where a good agreement between the experimental and numerical response in terms of initial stiffness, ultimate load and post ultimate response can be observed. Overall, best agreement between the numerical and the experimental results has been achieved for the t/100 imperfection magnitude which was adopted for the subsequent parametric studies. Finally, typical experimental and numerical failure modes are illustrated in Fig.11.

Table 6. Comparison of FE and test data

|	$F_{u,FE}/F_{u,test}$	$F_{u,FE}/F_{u,test}$	$F_{u,FE}/F_{u,test}$
Sections	t/10	t/50	t/100
3-point bending			
RHS $100 \times 50 \times 2$	1.04	1.05	1.05
RHS $100 \times 50 \times 3$	0.94	0.98	0.99
RHS $100 \times 50 \times 5$	0.88	0.93	0.94
RHS $100 \times 50 \times 3$-D	0.98	1.03	1.04
4-point bending			
RHS $100 \times 50 \times 2$	0.98	1.03	1.03
RHS $100 \times 50 \times 3$	0.92	0.97	0.98
RHS $100 \times 50 \times 5$	0.95	1.02	1.02
RHS $100 \times 50 \times 3$-D	0.97	0.99	0.99
Two-span continuous beams			
RHS $100 \times 50 \times 2$	0.91	0.92	0.92
RHS $100 \times 50 \times 3$	1.04	1.04	1.04
RHS $100 \times 50 \times 5$	0.89	0.90	0.91
RHS $100 \times 50 \times 3$-D	0.95	0.95	0.95
Mean	0.95	0.98	0.99
COV	0.05	0.05	0.05
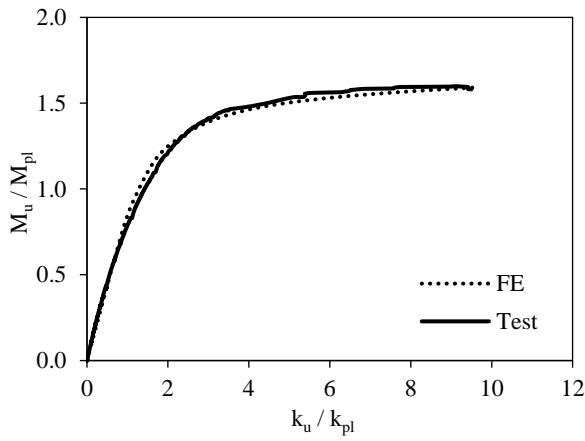
a) Simply-supported beams
(RHS $100 \times 50 \times 5$ – 4-point bending)
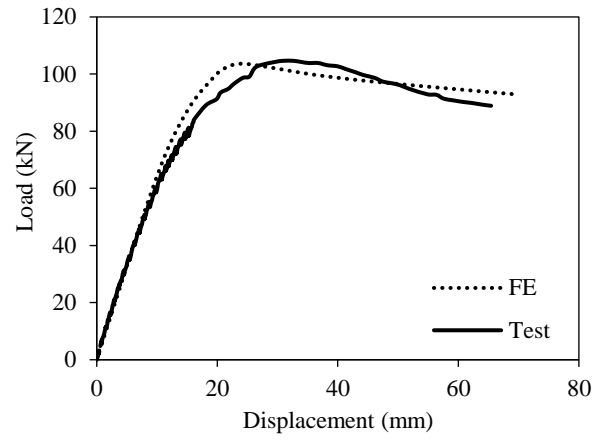
b) Continuous beams (RHS $100 \times 50 \times 3$-D)

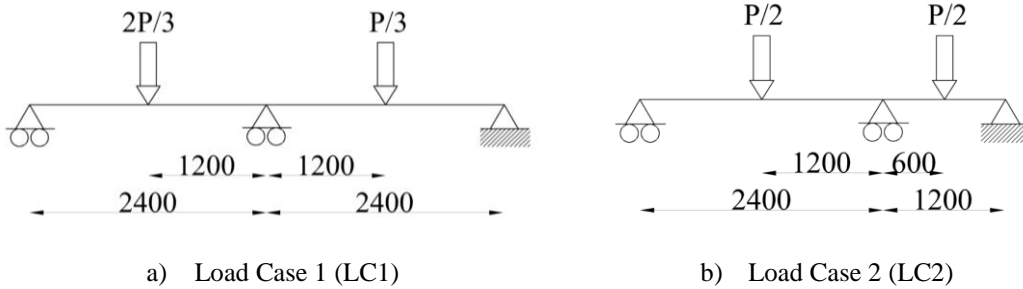**Fig.10. Typical experimental and numerical load-deformation response**
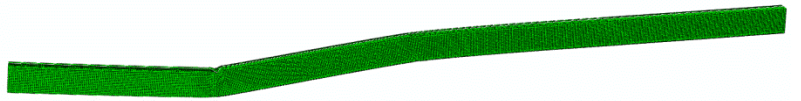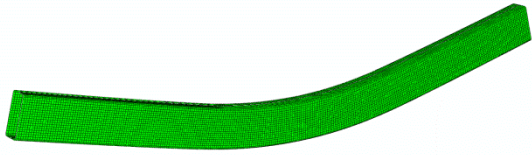
a) Simply-supported beams
(RHS $100 \times 50 \times 5$ – 4-point bending)

b) Continuous beams (RHS $100 \times 50 \times 3$-D)

Fig.11. Typical experimental and numerical failure modes

3.3   Parametric studies

Having established the ability of the FE models to accurately replicate the experimental response, parametric studies were conducted to expand the available structural performance data for various geometric parameters, such as cross-sectional slenderness, cross-section aspect ratio and loading arrangements. Three cross-sections aspect ratios, namely 1.0, 2.0 and 2.44, four thicknesses, namely 2 mm, 3 mm, 4 mm and 5 mm, two materials, namely austenitic and duplex and two-span load cases, as shown schematically in Fig.12, were considered. The obtained results are analysed and discussed in the following section.

a) Load Case 1 (LC1)

b) Load Case 2 (LC2)

Fig.12. Load Cases considered in the parametric studies (dimensions in mm)

4   Results and discussion

On the basis of the obtained experimental and numerical results, the Eurocode design provisions (EC3) [5] and the Continuous Strength Method (CSM) [15, 19] for the design of simply-supported and continuous beams are assessed.

4.1   The Eurocode design provisions

4.1.1 Simply-supported beams

EN 1993-1-4+A1 [5] adopts the cross-section classification procedure for the treatment of local buckling of stainless steel sections. According to EN 1993-1-4+A1 [5], Class 3 sections can reach their yield stress before the appearance of local buckling. The cross-sections which are capable of reaching their full plastic moment capacity are classified as Class 2 sections, while the Class 1 sections are characterized by their capability to reach and maintain their plastic moment resistance with sufficient deformation capacity and can therefore be used in plastic design. The classes of the tested cross-sections are shown in Table 7. Given that the present paper focuses on the plastic design of indeterminate structures, most of the specimens have been selected to be Class 1, while only the specimen with a nominal thickness of 2 mm is marginally classified as Class 2.

The experimental results of the 3-point and 4-point bending tests are used to assess the current Eurocode slenderness limits for internal elements in compression as well as the codified predicted capacities. Hence, the ratio of the moment resistance predicted by Eurocode (i.e. M_{pl} for Class 1 and 2 sections) normalized by the ultimate moment M_u is shown in Table 7. As can be seen, Eurocode predictions appear rather conservative and largely scattered. This owes to the fact that the strain-hardening exhibited by stocky stainless steel sections is not accounted for by Eurocode.

Table 7. Assessment of design methods for simply-supported beams

| Cross-section | Test configuration | EC3 [5] | | CSM [15] | |
		Class	M_{pl}/M_u	$\overline{\lambda}_{cs}$	M_{csm}/M_u
RHS 100 × 50 × 2	3-point bending	2	1.04	0.58	1.03
RHS 100 × 50 × 3		1	0.78	0.39	0.89
RHS 100 × 50 × 5		1	0.55	0.23	0.81
RHS 100 × 50 × 3-D		1	0.83	0.44	0.95
RHS 100 × 50 × 2	4-point bending	2	0.91	0.58	0.90
RHS 100 × 50 × 3		1	0.80	0.39	0.91
RHS 100 × 50 × 5		1	0.61	0.23	0.90
RHS 100 × 50 × 3-D		1	0.83	0.44	0.94
Mean			0.79		0.92
COV			0.20		0.07

In Fig.13(a), the ultimate moment M_u normalized by the plastic moment M_{pl} is plotted against the flange slenderness $c/t\varepsilon$, where c and t the plate's width and thickness respectively and $\varepsilon=[(235/\sigma_{0.2})(E/210000)]^{1/2}$ with $\sigma_{0.2}$ and E as previously defined. The Class 2 limit of 35 is also specified, showing that the current limit is acceptable. In order to assess Class 1 limit, the deformation capacity R of the specimens that have failed upon reaching M_{pl} is plotted against the flange slenderness in Fig.13(b). The current Class 1 limit for the part of the specimen subjected to compression is 33. Note that no rules for plastic global analysis are given in Eurocode [5]. Hence there is an absence of codified deformation capacity requirement for Class 1 stainless steel cross-sections. Nevertheless, the deformation capacity requirement R=3 from carbon steel has been considered [29, 30]. As can be seen, most of the Class 1 specimens have reached beyond the required deformation capacity, while the cross-section 100×50×3 Duplex for 3-point bending test fell below the deformation

capacity requirement of 3. Overall the presented results show that the carbon steel limits could be adopted for stainless steel but further tests are required.

a) Class 2 limit

b) Class 1 limit
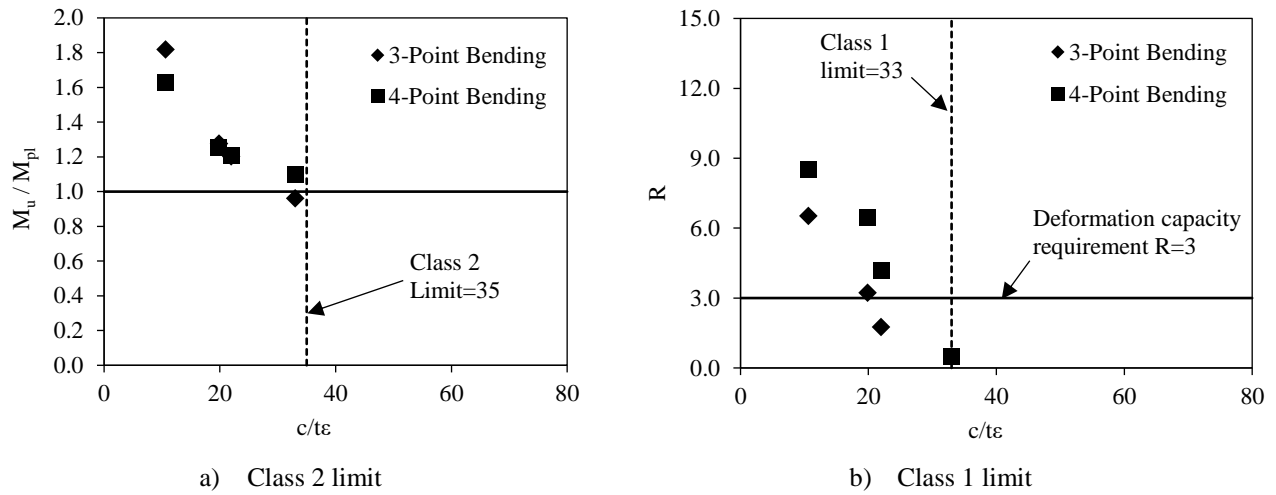
Fig.13. Assessment of the Eurocode slenderness limits for internal elements in compression [5]

4.1.2 Continuous beams

According to Eurocode [5], the ultimate load that a continuous beam can carry is the one that causes the bending moment of the most heavily stressed cross-section, as determined by elastic analysis, to reach its respective moment resistance (i.e. plastic moment resistance M_{pl} for Class 1 and 2 sections, elastic moment resistance M_{el} for Class 3 sections and effective moment resistance M_{eff} for Class 4 sections). The current provisions account neither for strain-hardening nor for moment redistribution and are expected to lead to overly conservative and scattered design predictions. In order to assess the applicability of traditional plastic design for Class 1 stainless steel sections, a variation of the current Eurocode method for carbon steel structures, which allows Class 1 sections to be plastically designed, assuming rigid-plastic material response, is also assessed herein. This method is expected to lead to improved predictions for Class 1 sections. The suitability of the two aforementioned methods, denoted as "EC3 no redistribution" and "EC3 with redistribution", is discussed in Section 4.3.

4.2 The Continuous Strength Method

4.2.1 Simply-supported beams

The Continuous Strength Method is a design method for the treatment of local buckling of stainless steel cross-sections, rationally accounting for the significant strain-hardening exhibited by stocky sections. The method is based on the experimentally derived base curve, which relates the non-dimensional slenderness $\overline{\lambda}_{cs}$ of a cross-section to its deformation capacity ε_{csm}, and is applicable to sections with $\overline{\lambda}_{cs} \leq 0.68$. Based on the deformation capacity and an assumed elastic-linear hardening material response, the ultimate moment resistance M_{csm} corresponding to the local buckling strain ε_{csm} is determined according to Equation (4) for RHS [15]

$$\frac{M_{csm}}{M_{pl}} = 1 + \frac{E_{sh}}{E}\frac{W_{el}}{W_{pl}}\left(\frac{\varepsilon_{csm}}{\varepsilon_y}-1\right) - \left(1-\frac{W_{el}}{W_{pl}}\right)\left(\frac{\varepsilon_{csm}}{\varepsilon_y}\right)^{-2} \hspace{2cm} (4)$$

where E_{sh} the strain-hardening slope, E the modulus of elasticity, W_{el} the elastic section modulus, W_{pl} the plastic section modulus, ε_{csm} the CSM predicted failure strain and ε_y the yield strain. The method and the relevant expressions are described in [15]. In order to assess the applicability of Equation (4) to the presently studied cross-sections, the results of the 3-point and 4-point bending tests are used. The CSM to ultimate moment ratios are reported in Table 7, where the effect of corner strength enhancements has been accounted for according to [26]. The corresponding non-dimensional slenderness $\overline{\lambda}_{cs}$, which is defined as $(\sigma_{0.2}/\sigma_{cr})^{1/2}$ where σ_{cr} is the elastic critical buckling stress of the cross-sections that has been evaluated

from the analytical formuli provided in [31], is also included. As expected, the application of the CSM, which rationally accounts for the pronounced strain-hardening in the material response of stainless steels, leads to more accurate design predictions compared to those of Eurocode.

4.2.2 Continuous beams

Based on the original CSM, the strain-hardening of the most heavily stressed cross-section of an indeterminate structure is accounted for, but no moment redistribution is allowed. Hence, the method is expected to provide improved ultimate capacity predictions compared to the Eurocode method.

An attempt was made to extend the CSM to indeterminate carbon steel structures [32] and stainless steel structures [19], by allowing for moment redistribution in a similar way with the traditional plastic analysis procedure, but adopting an elastic-linear hardening material response rather than the traditional rigid-plastic material response. In order to determine the design strengths of indeterminate stainless steel structures based on the CSM design procedure, the following six steps are required:

1. Similar to traditional plastic design, the identification of the location of the i plastic hinges at collapse and the determination of the respective hinge rotations ϑ_i are initially required.

2. The maximum strain (ε_{csm}) that a cross-section can undergo according to its slenderness and the base curve are then evaluated based on Equation (5).

$$\left(\frac{\varepsilon_{csm}}{\varepsilon_y}\right)_i = \frac{0.25}{\left(\bar{\lambda}_{cs}\right)_i^{3.6}} \text{ but } \left(\frac{\varepsilon_{csm}}{\varepsilon_y}\right)_i \leq \min\left(15; \frac{0.1\varepsilon_u}{\varepsilon_y}\right) \text{ for } \left(\bar{\lambda}_{cs}\right)_i \leq 0.68 \tag{5}$$

where ε_{csm} is the maximum attainable strain, which takes place afore the occurrence of local buckling, ε_y the yield strain, λ_{cs} the non-dimensional cross-sectional slenderness and ε_u the strain at ultimate tensile stress.

3. For each collapse mechanism, the rotation demand α_i of each of the i hinges needs to be determined according to Equation (6).

$$\alpha_i = \frac{\theta_i h_i}{\left(\varepsilon_{csm}/\varepsilon_y\right)_i} \tag{6}$$

where θ_i is the relative rotation derived from kinematics considerations for the collapse mechanism considered, h_i the section height at the considered location and $\varepsilon_{csm}/\varepsilon_y$ the corresponding normalized strain ratio at the hinge.

4. The deformation demands in terms of strains at other plastic hinges locations are then assigned relative to that of the critical hinge from Equation (7).

$$\left(\frac{\varepsilon_{csm}}{\varepsilon_y}\right)_i = \frac{\alpha_i}{\alpha_{crit}}\left(\frac{\varepsilon_{csm}}{\varepsilon_y}\right)_{crit} \leq \left(\frac{\varepsilon_{csm}}{\varepsilon_y}\right)_i \tag{7}$$

5. Then the cross-section bending moment capacity M_i at each plastic hinge on the corresponding strain ratio $(\varepsilon_{csm}/\varepsilon_y)_i$ is calculated based on the Equation (4).

6. Finally, the collapse load of the system is determined by equating the external work done by the applied load F_j to the internal work resulting from the hinge rotations according to Equation (8).

$$\Sigma_j F_j \delta_j = \Sigma_i M_i \theta_i \tag{8}$$

Both aforementioned methods, namely the "CSM no redistribution" and the "CSM with redistribution", are assessed in Section 4.3. Note that the latter is considered only when the $\varepsilon_{csm}/\varepsilon_y$ ratio has a minimum value of 3.6 for box-sections and 3 for I-sections [19, 32].

4.3   Discussion

In this section, the design methods for the performance and design of stainless steel continuous beams are discussed. In particular, the ultimate capacity predictions (F_{pred}) determined according to the four design methods outlined in Sections 4.1.2 and 4.2.2 are normalized by the ultimate experimental loads and the results are reported in Table 8. Aiming to allow a general overview of plastic design of stainless steel structures, test data reported in literature [17-20] are also considered. It can be seen that the Eurocode method, which allows for neither moment redistribution nor strain-hardening yields the most conservative design predictions. Improved design predictions are obtained for both the variation of the Eurocode, which allows for moment redistribution and the CSM without moment redistribution. Overall both the effect of strain-hardening and moment redistribution have to be taken into account, in order to obtain accurate predictions of the observed response and as expected the CSM with moment redistribution results in the most accurate (mean F_{pred}/F_u closer to 1) and consistent (small COV) design predictions. It should be noted that the CSM for indeterminate structures seems better suited for austenitic and duplex grades compared to the ferritic ones.

Similar conclusions are drawn from the results of the numerical parametric studies shown in Table 9 and Fig.14 for the two load cases considered. More conservative design predictions can be observed for the EC3 methods. This issue is overcome by the CSM rational exploitation of the material strain-hardening. In both considered structural configurations, significantly improved predicted capacities in terms of both efficiency and consistency are evident by the CSM considering plastic design. It is noteworthy that similar findings were reported at a recent numerical study [33] that rigorously investigated the response of continuous stainless steel beams in five different structural configurations. It can be concluded that the CSM for indeterminate structures sufficiently addresses the issue of both strain-hardening at cross-section level and moment redistribution at structural level.

a)   LC1   b)   LC2
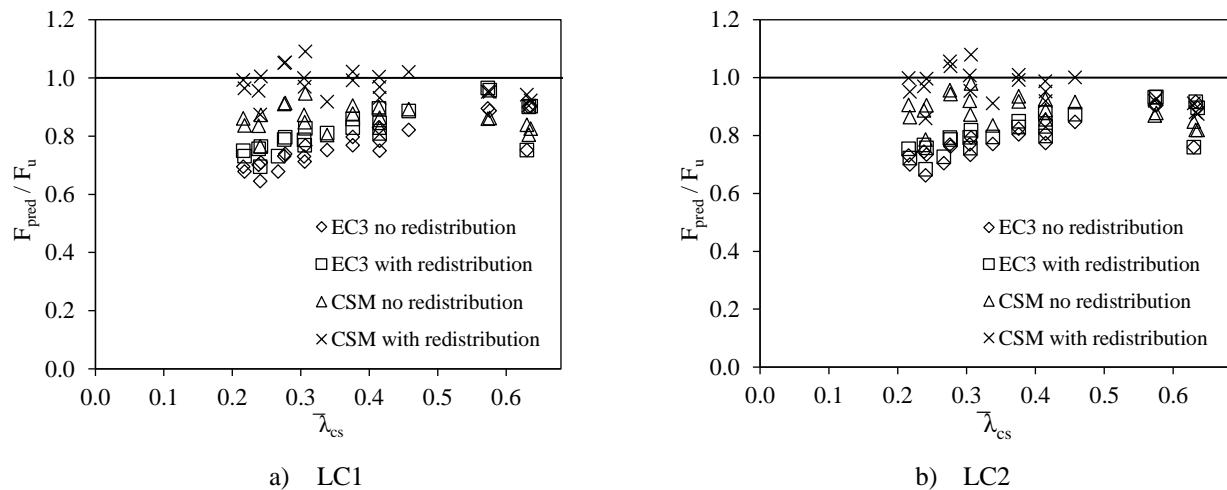
Fig.14. Parametric Studies

Table 8. Assessment of design methods for stainless steel continuous beams – Experimental results

	Specimen	Grade	Class	EC3 no redistribution	EC3 with redistribution	CSM no redistribution	CSM with redistribution
				F_{pred}/F_u			
[17, 18]	SHS 80 × 80 × 3	1.4301	2	0.74	0.74	0.76	N/A
	SHS 80 × 80 × 3	1.4301	2	0.80	0.80	0.82	N/A
	RHS 120 × 80 × 4	1.4301	1	0.72	0.81	0.80	0.89
	RHS 120 × 80 × 4	1.4301	1	0.72	0.81	0.80	0.89
	I-100 × 100 × 8	1.4306	1	0.70	0.79	0.89	1.00
[19]	SHS 50 × 50 × 3	1.4301/1.4307	1	0.60	0.68	0.81	0.91
	SHS 50 × 50 × 3	1.4301/1.4307	1	0.49	0.68	0.67	0.91
	SHS 60 × 60 × 3	1.4301/1.4307	1	0.64	0.72	0.83	0.93
	SHS 60 × 60 × 3	1.4301/1.4307	1	0.67	0.76	0.87	0.98
	SHS 100 × 100 × 3	1.4301/1.4307	4	0.71	0.71	0.85	N/A
	SHS 100 × 100 × 3	1.4301/1.4307	4	0.72	0.72	0.85	N/A
	RHS 60 × 40 × 3	1.4301/1.4307	1	0.56	0.63	0.75	0.84
	RHS 60 × 40 × 3	1.4301/1.4307	1	0.56	0.63	0.75	0.85
	RHS 60 × 40 × 3	1.4301/1.4307	1	0.61	0.69	0.75	0.84
	RHS 60 × 40 × 3	1.4301/1.4307	1	0.51	0.71	0.62	0.85
	I-200 × 140 × 6 × 6	1.4162	4	0.68	0.68	0.76	N/A
	I-200 × 140 × 8 × 6	1.4162	3	0.66	0.66	0.74	N/A
	I-200 × 140 × 10 × 8	1.4162	1	0.70	0.79	0.81	0.91
	I-200 × 140 × 12 × 8	1.4162	1	0.64	0.72	0.83	0.93
	I-200 × 140 × 6 × 6	1.4162	4	0.56	0.56	0.62	N/A
	I-200 × 140 × 8 × 6	1.4162	3	0.57	0.57	0.65	N/A
	I-200 × 140 × 10 × 8	1.4162	1	0.60	0.84	0.70	0.95
	I-200 × 140 × 12 × 8	1.4162	1	0.59	0.82	0.77	1.02
[20]	SHS 80 × 80 × 4	1.4003	1	1.06	1.20	1.07	1.20
	SHS 80 × 80 × 4	1.4003	1	1.04	1.18	1.05	1.18
	SHS 60 × 60 × 3	1.4003	1	0.95	1.08	0.97	1.09
	RHS 80 × 40 × 4	1.4003	1	0.92	1.04	0.95	1.07
	RHS 80 × 40 × 4	1.4003	1	0.91	1.03	0.91	1.03
	RHS 120 × 80 × 3	1.4003	3	1.06	1.06	N/A	N/A
	RHS 120 × 80 × 3	1.4003	4	0.85	0.85	N/A	N/A
	RHS 70 × 50 × 2	1.4003	1	0.98	1.11	0.94	N/A
	RHS 70 × 50 × 2	1.4003	4	0.77	0.77	N/A	N/A
	RHS 100 × 50 × 2	1.4301/1.4307	2	0.94	0.94	0.93	N/A
	RHS 100 × 50 × 3	1.4301/1.4307	1	0.90	0.97	1.02	1.13
	RHS 100 × 50 × 5	1.4301/1.4307	1	0.55	0.59	0.70	0.81
	RHS 100 × 50 × 3	1.4462	1	0.81	0.87	0.89	0.99
Mean		Ferritic		0.95	1.04	0.98	1.11
COV				0.10	0.14	0.07	0.07
Mean		Duplex		0.65	0.72	0.75	0.96
COV				0.12	0.16	0.11	0.05
Mean		Austenitic		0.67	0.74	0.80	0.91
COV				0.18	0.13	0.12	0.09
Mean		All		0.74	0.81	0.82	0.97
COV				0.22	0.21	0.14	0.12

Table 9. Assessment of design methods for stainless steel continuous beams – Numerical results

	Specimen	Grade	Number of FE	EC3 no redistribution	EC3 with redistribution	CSM no redistribution	CSM with redistribution
				F_{pred}/F_u			
LC1	50×50 (H/B=1.0)	1.4301/1.4307	4	0.77	0.83	0.88	1.01
	50×50 (H/B=1.0)	1.4462	4	0.77	0.81	0.84	0.96
	100×50 (H/B=2.0)	1.4301/1.4307	4	0.78	0.84	0.88	1.01
	100×50 (H/B=2.0)	1.4462	4	0.76	0.80	0.82	0.94
	122×50 (H/B=2.44)	1.4301/1.4307	4	0.76	0.81	0.89	1.03
	122×50 (H/B=2.44)	1.4462	4	0.75	0.79	0.86	0.97
LC2	50×50 (H/B=1.0)	1.4301/1.4307	4	0.80	0.83	0.91	1.02
	50×50 (H/B=1.0)	1.4462	4	0.80	0.81	0.87	0.97
	100×50 (H/B=2.0)	1.4301/1.4307	4	0.80	0.82	0.90	1.00
	100×50 (H/B=2.0)	1.4462	4	0.78	0.80	0.84	0.92
	122×50 (H/B=2.44)	1.4301/1.4307	4	0.79	0.80	0.91	1.02
	122×50 (H/B=2.44)	1.4462	4	0.77	0.79	0.88	0.95
Mean		All	48	0.78	0.81	0.87	0.99
COV				0.09	0.09	0.05	0.05

5   Conclusions

The structural performance and plastic design of stainless steels have been studied in this paper. Eight experiments on simply-supported beams employing austenitic and duplex stainless steels and four experiments on continuous beams of the same material have been performed. Finite element models were developed and the results of the numerical analyses were compared with the experimental ones. Parametric studies were then conducted in order to investigate the response of continuous beams over a wide range of cross-section slendernesses, aspect ratios and span lengths. Based on the obtained results, the Eurocode design provisions [5] and the strain-based design approach termed continuous strength method [15] were assessed. It was shown that the current Eurocode approach [5] underestimates the strength of stainless continuous beams. This is because the formation of successive plastic hinges and the moment redistribution in indeterminate structures with adequate deformation capacity, as well as the effect of strain-hardening at cross-sectional level, are not accounted for. Based on collated test data on continuous stainless steel beams [17-20] and the experimental and numerical results of the present study, it was shown that accounting for both the strain-hardening and the moment redistribution is of paramount importance for the design. To this end, the continuous strength method, which rationally accounts for the local buckling at cross-section level, extended to the design of stainless steel indeterminate structures in order to consider the moment redistribution, provides the most accurate design estimations. Further research is underway to extend the method to the design of stainless steel frames.

References

[1] Baddoo N.R. Stainless steel in construction: A review of research, applications, challenges and opportunities. Journal of Constructional Steel Research 64(11):1199-1206, 2008.

[2] Gedge G. Structural uses of stainless steel - buildings and civil engineering. Journal of Constructional Steel Research 64(11):1194-1198, 2008.

[3] Gardner L., Cruise R.B., Sok C.P., Krishnan K. and Ministro Dos Santos J. Life-cycle costing of metallic structures. Engineering Sustainability 160(4):167-177, 2007.

[4] Rossi B. Discussion on the use of stainless steel in construction in view of sustainability. Thin-Walled Structures 83:182-189, 2014.

[5] EN 1993-1-4+A1. Eurocode 3: Design of steel structures - Part 1.4: General rules - Supplementary rules for stainless steel. CEN, 2015.

[6] AS/NZS 4673. Cold-formed stainless steel structures. AS/NZS4673. Sydney: Standards Australia, 2001.

[7] SEI/ASCE 8-02. Specification for the design of cold-formed stainless steel structural members. American Society of Civil Engineers (ASCE), 2002.

[8] AISC Design Guide 27. Structural Stainless Steel. American Institute of Steel Construction, 2013.

[9] Rasmussen K.J.R. and Hancock G.J. Design of cold-formed stainless steel tubular members II: Beams. Journal of Structural Engineering ASCE 119(8):2368-2386, 1993.

[10] Young B. and Lui W.M. Behavior of cold-formed high strength stainless steel sections. Journal of Structural Engineering ASCE 131(11):1738-1745, 2005.

[11] Zhou F. and Young B. Tests of cold-formed stainless steel tubular flexural members. Thin-Walled Structures 43(9):1325-1337, 2005.

[12] Zhao O., Rossi B., Gardner L. and Young B. Behaviour of structural stainless steel cross-sections under combined loading - Part I: Experimental study. Engineering Structures 89: 236-246, 2015.

[13] Gardner L. and Nethercot D.A. Experiments on stainless steel hollow sections - Part 2: Member behaviour of columns and beams. Journal of Constructional Steel Research 60(9):1319-1332, 2004.

[14] Gardner L. and Theofanous M. Discrete and continuous treatment of local buckling in stainless steel elements. Journal of Constructional Steel Research 64(11):1207-1216, 2008.

[15] Afshan S. and Gardner L. The continuous strength method for structural stainless steel design. Thin-Walled Structures 68: 42-49, 2013.

[16] Becque J., Lecce M. and Rasmussen K.J.R. The direct strength method for stainless steel compression members. Journal of Constructional Steel Research 64(11):1231-1238, 2008.

[17] Mirambell E. and Real E. On the calculation of deflections in structural stainless steel beams: an experimental and numerical investigation. Journal of Constructional Steel Research 54(1):109-133, 2000.

[18] Real E. and Mirambell E. Flexural behaviour of stainless steel beams. Engineering Structures 27(10):1465-1475, 2005.

[19] Theofanous M., Saliba N., Zhao O. and Gardner L. Ultimate response of stainless steel continuous beams. Thin-Walled Structures 83:115-157, 2014.

[20] Arrayago I. and Real E. Experimental study on ferritic stainless steel simply supported and continuous beams. Journal of Constructional Steel Research 119:50-62, 2016.

[21] Arrayago I., Real E. and Mirambell E. Design of stainless steel continuous beams with tubular cross-sections. Engineering Structures 151:422-431, 2017.

[22] Theofanous M. and Gardner L. Experimental and numerical studies of lean duplex stainless steel beams. Journal of Constructional Steel Research 66(6):816-825, 2010.

[23] BS EN ISO 6892-1. British standard: metallic materials – tensile testing. Part 1: Method of test at ambient temperature. The Standards Policy and Strategy Committee, 2009.

[24] Rasmussen KJR. Full-range stress-strain curves for stainless steel alloys. Journal of Constructional Steel Research 59(1):47-61, 2003.

[25] Gardner L and Nethercot DA. Experiments on stainless steel hollow sections - Part 1: Material and cross-sectional behaviour. Journal of Constructional Steel Research 60(9):1291-1318, 2004.

[26] Cruise R.B. and Gardner L. Strength enhancements induced during cold forming of stainless steel sections. Journal of Constructional Steel Research 64(11):1310-1361, 2008.

[27] Bock M., Arrayago I., Real E. and Mirambell E. Study of web crippling in ferritic stainless steel cold formed sections. Thin-Walled Structures 69:29-44, 2013.

[28] Hibbitt, Karlsson, Sorensen Inc. ABAQUS/Standard user's manual. Version 6.10, USA: Pawtucket, 2010.

[29] Bild S., Roik K., Sedlacek G., Stutzki C. and Spangemacher R. The b/t-ratios controlling the applicability of analysis models in Eurocode 3, Part 1.1. Background Document, 5, 1989.

[30] Sedlacek G. and Feldmann M. The b/t-ratios controlling the applicability of analysis models in Eurocode 3, Part 1.1. Background Document, 5, 1995.

[31] Seif M. and Schafer B.W. Local buckling of structural steel shapes. Journal of Constructional Steel Research 66(10):1232-1247, 2010.

[32] Gardner L., Wang F.C. and Liew A. Influence of strain hardening on the behaviour and design of steel structures, International Journal of Structural Stability and Dynamics 11(5): 855–75, 2011.

[33] Kokosis G., Gkantou M. and Theofanous M. Ultimate response and design of stainless steel continuous beams. In Proceedings of the 8th European Conference on Steel and Composite Structures. Copenhagen (Denmark). September 13–15 2017.